European Conference on Computational Fluid Dynamics
ECCOMAS CFD 2006
P. Wesseling, E. Oñate and J. Périaux (Eds)
© TU Delft, The Netherlands, 2006

ON FINITE ELEMENT METHOD APPLICATION IN COMPUTATIONAL AEROELASTICITY

Petr Sváček*, Jaromír Horáček†

* Czech Technical University, Faculty of Mechanical Engineering,
Karlovo nám. 13, Praha 2, 121 35
e-mail: *Petr.Svacek@fs.cvut.cz*
† Czech Academy of Sciences, Institute of Thermomechanics,
Dolejskova 5, 182 00 Praha 8

Key words: aeroelasticity, finite element method

Abstract. *The paper focuses on numerical simulations of coupled fluid and structural models of aeroelasticity. The fluid motion is described by the incompressible Reynolds Averaged Navier-Stokes equations (RANS) coupled with Spallart-Almaras turbulence model. The numerical solution by finite element method (FEM) stabilized with the Galerkin Least Squares (GLS) method is applied onto RANS system of equations. The Spallart- Almaras turbulence model is approximated by the FEM stabilized by the streamline upwind/Petrov-Galerkin (SUPG) method. The airfoil motion is described by a system of ordinary differential equations. The airfoil vibrations with large amplitudes result in deformations of the computational domain, which are treated with the aid of Arbitrary Lagrangian-Eulerian(ALE) method. Numerical results for several problems are compared to NASTRAN computations as well as to available experimental data.*

1 INTRODUCTION

The paper is focused on numerical simulations of two dimensional viscous incompressible air flow around an airfoil. The main objective is a correct numerical approximation of aerodynamic forces acting on the oscillating airfoil as well as the numerical simulations of aeroelastic phenomena in postcritical regimes after losing the stability of the system. The relevant flow velocities for the selected class of problems are in the range $0 - 120$ m s^{-1}. The flow is described by the incompressible Navier-Stokes equations, where the turbulence effects are taken into account.

The numerical approximation of the incompressible flow can be carried out with the use of various methods. Here the FE method is used for the spatial discretization of the problem. Several sources of numerical instabilities have to be treated. The finite elements for velocity and pressure need to be selected to satisfy the Babuška-Brezzi condition in order to guarantee the stability of the scheme. Furthermore, very high Reynolds numbers result in the appearance of spurious oscillations in the approximate solution. Here,

the stabilization based on GLS (Galerkin Least-Squares) method together with grad-div stabilization is employed. The choice of the stabilization parameters is based on the numerical analysis of the problem as well as the numerical experience, see [5], [8]. The method is applied to the solution of Reynolds Averaged Navier-Stokes (RANS) equations. The Reynolds stresses involved in the RANS equations are modelled with the aid of the Spallart-Almaras turbulence model (for an overview of turbulence models used in computational fluid dynamics (CFD), see, e.g. [10]).

The structure motion is simulated by the solution of a system of nonlinear ordinary differential equations for the vertical and angular displacements. The airfoil motion results in deformations of the computational domain, which are treated with the aid of Arbitrary Lagrangian-Eulerian(ALE) method, see [6], [4].

2 PROBLEM DESCRIPTION

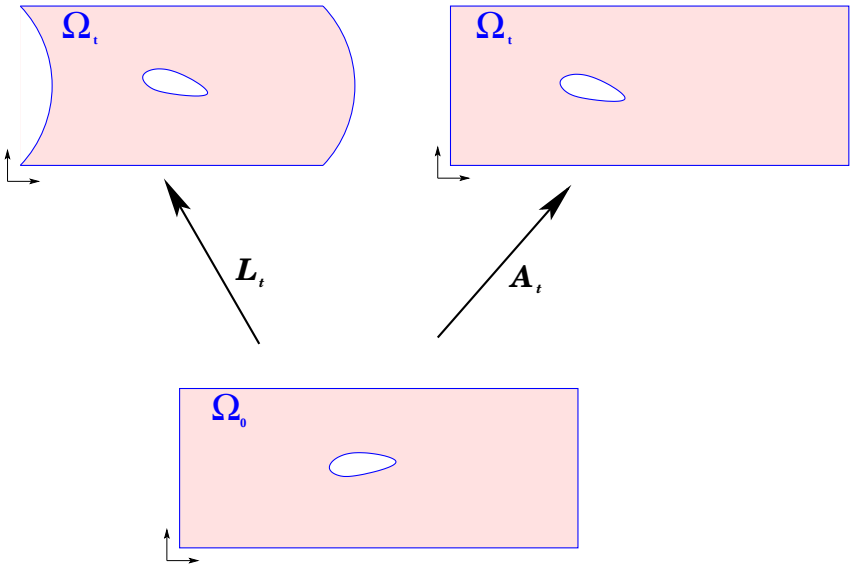


Figure 1: Comparison of Lagrangian and Arbitrary Lagrangian-Eulerian mappings.
In this figure the demonstration of Lagrangian mapping (on the left) and ALE mapping (on the right) is shown. Although the Lagrangian mapping allows the structure to be deformed, the other (artificial) boundaries are also deformed , which is unusable in practical computations. ALE mapping is then the "compromise" between having fixed artificial boundaries and deformed structure boundary.

2.1 NUMERICAL SIMULATION ON MOVING MESHES

The numerical approximation of the time derivative by a time difference leads to complications in the case of moving meshes. With the use of Arbitrary Lagrangian-Eulerian (ALE) method the original mathematical model can be reformulated in a suitable way and the finite element space discretization together with a suitable time discretization can

be introduced. The ALE method is based on the definition of an ALE mapping of the original configuration computational domain $\mathcal{G}_0$ onto the computational domain $\mathcal{G}_t$ and the definition of the ALE domain velocity as the time derivative of the ALE mapping $\mathcal{A}_t$, i.e.

$$\mathcal{A}_t : \mathcal{G}_0 \mapsto \mathcal{G}_t, \qquad \tilde{\mathbf{w}}_g = \frac{\partial \mathcal{A}_t}{\partial t}, \qquad \mathbf{w}_g = \tilde{\mathbf{w}}_g \circ \mathcal{A}_t^{-1}.$$

With the aid of the time differentiation with respect to the original configuration $\mathcal{G}_0$, leading to the so-called ALE derivative denoted by $\frac{D^{\mathcal{A}_t}}{Dt}$, the time derivative of any function can be rewritten as $\frac{\partial}{\partial t} = \frac{D^{\mathcal{A}_t}}{Dt} - (\mathbf{w}_g \cdot \nabla)$. For more details about ALE method, see, e.g., [6].

2.2 REYNOLDS AVERAGED NAVIER-STOKES EQUATIONS AND TURBULENCE MODELLING

Let us assume that at each time instant t the boundary $\mathcal{G}_t$ is split into three distjoint parts $\partial\mathcal{G}_t = \Gamma_D \cup \Gamma_O \cup \Gamma_{W_t}$. The fluid velocity vector $\mathbf{v} = (v_1, v_2)$ is decomposed into mean part $\mathbf{V} = (V_1, V_2)$ and fluctuating part $\mathbf{v}' = (v_1', v_2')$, i.e. $\mathbf{v} = \mathbf{V} + \mathbf{v}'$. Similary the kinematic pressure p is decomposed into mean part P and fluctuating part p', i.e. $p = P + p'$. The Reynolds Averaged Navier-Stokes system of equations reads

$$\frac{\partial V_i}{\partial t} - \nu \sum_j \frac{\partial}{\partial x_j}\left(\frac{\partial V_i}{\partial x_j} + \frac{\partial V_j}{\partial x_i}\right) + (\mathbf{V}\cdot\nabla)\, V_i + \frac{\partial P}{\partial x_i} = -\sum_j \frac{\partial}{\partial x_j}\overline{v_i' v_j'} + f_i, \qquad (1)$$

$$\nabla \cdot \mathbf{V} = 0,$$

where in the right hand side terms are so called Reynolds stresses $\sigma_{ij} = -\overline{v_i' v_j'}$.

The system (1) is equipped with the boundary conditions

$$\begin{aligned} &\text{a)} \quad \mathbf{V} = \mathbf{V}_D, \qquad \text{on } \Gamma_D, \\ &\text{b)} \quad \mathbf{V} = \mathbf{w}_g, \qquad \text{on } \Gamma_{W_t}, \\ &\text{c)} \quad -\nu \sum_j \left(\frac{\partial V_i}{\partial x_j} + \frac{\partial V_j}{\partial x_i}\right)\mathbf{n}_j + (P - P_{ref})\mathbf{n}_i = \sum_j \sigma_{ij}\mathbf{n}_j, \qquad \text{on } \Gamma_O, \end{aligned} \qquad (2)$$

where $\mathbf{w}_g$ is the ALE domain velocity, $\mathbf{V}_D$ is Dirichlet boundary condition and P_{ref} is the reference pressure at the outlet. By $\mathbf{n} = (\mathbf{n}_1, \mathbf{n}_2)$ we denote the unit outward normal to the boundary of the domain. If we set $\sigma_{ij} \equiv 0$, then the boundary condition (2,c) is reduced to the well-known "do-nothing" boundary condition. Further, for the system of equations (1) we use the initial condition $\mathbf{V}(x, 0) = \mathbf{V}_0(x)$ for $x \in \mathcal{G}_0$.

The Reynolds stress tensor $\sigma = (\sigma_{ij})$ requires further modelling. We use the Bousinesq assumption consisting of taking σ in the form

$$\sigma_{ij} = -\frac{2}{3}k\delta_{ij} + \nu_T\left(\frac{\partial V_i}{\partial x_j} + \frac{\partial V_j}{\partial x_i}\right),$$

where k is the kinetic energy of the fluctuating parts of velocity vector and ν_T is turbulent kinematic viscosity.

The turbulent kinematic viscosity is modelled with the aid of one-equation Spallart-Almaras model, the volumetric part $-\frac{2}{3}k\delta_{ij}$ is included in the pressure term. In this approach, the system of equations (1) is coupled with the following nonlinear partial differential equation

$$\frac{D^{\mathcal{A}_t}\tilde{\nu}}{Dt} + ((\mathbf{V}-\mathbf{w}_g)\cdot\nabla)\,\tilde{\nu} = \frac{1}{\beta}\left[\sum_{i=1}^{2}\frac{\partial}{\partial x_i}\left((\nu+\tilde{\nu})\frac{\partial\tilde{\nu}}{\partial x_i}\right) + c_{b_2}\left(\nabla\tilde{\nu}\right)^2\right] + G - Y, \quad (3)$$

equipped with the boundary conditions $\tilde{\nu} = 0$ on Γ_{W_t} and $\frac{\partial\tilde{\nu}}{\partial\mathbf{n}} = 0$ on $\Gamma_O \cup \Gamma_D$. The functions G and Y are functions of the tensor of rotation $\Omega = \Omega(\mathbf{V})$ of the mean velocity vector $\mathbf{V}$ and of the wall distance y, i.e.

$$G = c_{b_1}\tilde{S}\cdot\tilde{\nu}, \quad Y = c_{w_1}\frac{\tilde{\nu}^2}{y^2}\left(\frac{1+c_{w_3}^6}{1+c_{w_3}^6/g^6}\right)^{\frac{1}{6}}, \quad \tilde{S} = \left(S + \frac{\tilde{\nu}}{\kappa^2 y^2}f_{v_2}\right), \quad f_{v_2} = 1 - \frac{\chi}{1+\chi f_{v_1}},$$
$$g = r + c_{w_2}(r^6 - r), \quad r = \frac{\tilde{\nu}}{\tilde{S}\kappa^2 y^2}, \quad S = \sqrt{2\Omega(\mathbf{V}):\Omega(\mathbf{V})}, \quad \Omega(\mathbf{V}) = \tfrac{1}{2}(\nabla\mathbf{V} - \nabla\mathbf{V}^T).$$

The following choice of constants is used $c_{b_1} = 0.1355$, $c_{b_2} = 0.622$, $\beta = \frac{2}{3}$, $c_v = 7.1$, $c_{w_3} = 0.3$, $c_{w_3} = 2.0$, $\kappa = 0.41$, $c_{w_1} = c_{b_1}/\kappa^2 + (1+c_{b_2})/\beta$. The Reynolds stresses then are computed as

$$\sigma_{ij} = -\nu_T\left(\frac{\partial V_i}{\partial x_j} + \frac{\partial V_j}{\partial x_i}\right), \quad \nu_T = \tilde{\nu}\frac{\chi^3}{\chi^3 + c_v^3}, \quad \chi = \frac{\tilde{\nu}}{\nu},$$

where the volumetric part of σ has been included in the pressure term, i.e. $P^* = P + \frac{2}{3}k$. In what follows we shall not distinguish between P and P^*, we shall simply use the symbol P.

The space discretization of the problem is carried out by the finite element method, which starts from the so called weak formulation. To this end we introduce the velocity spaces W, X, the pressure space Q and the turbulence model space Λ:

$$W = (H^1(\mathcal{G}_t))^2, \quad X = \{\boldsymbol{\eta}\in W; \boldsymbol{\eta}|_{\Gamma_D\cup\Gamma_{Wt}} = 0\}, \quad Q = L^2(\mathcal{G}_t), \quad \Lambda = \{\phi\in W; \phi|_{\Gamma_{Wt}} = 0\}$$

where $L^2(\mathcal{G}_t)$ is the Lebesgue space of square integrable functions over the domain $\mathcal{G}_t$ and $H^1(\mathcal{G}_t)$ is the Sobolev space of functions square integrable together with their first order derivatives.

Now, by multiplying the system of equation (1) by a test function $\boldsymbol{\eta}\in X$ and $q\in Q$, integrating over the domain $\mathcal{G}_t$ and using Green's theorem, we obtain the weak formulation: find $\mathbf{V}: \langle 0,T\rangle \mapsto W$ such that for all t the Dirichlet boundary conditions (2 a-b) are satisfied and $P: \langle 0,T\rangle \mapsto Q$ such that for all $t\in\langle 0,T\rangle$ the following equality holds

$$\mathbf{a}(\mathbf{V}-\mathbf{w}_g; \mathbf{V}, P; \boldsymbol{\eta}, q) = \mathbf{L}(\boldsymbol{\eta}), \qquad \text{for all } \boldsymbol{\eta}\in X, q\in Q \quad (4)$$

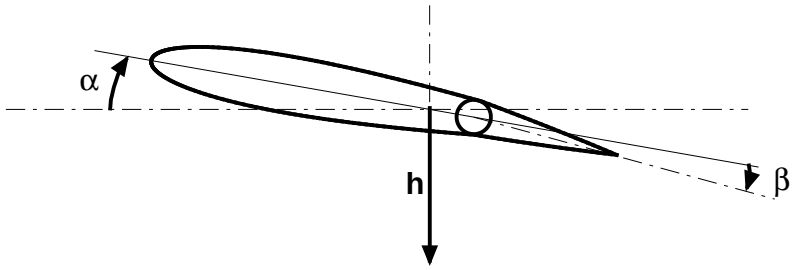


Figure 2: Airfoil pitching, plunging and rotation of the flap

where

$$\begin{aligned}\mathbf{a}(\mathbf{b};\mathbf{V},P;\boldsymbol{\eta},q) &= \left(\frac{D^{\mathcal{A}_t}\mathbf{V}}{Dt}+(\mathbf{b}\cdot\nabla)\mathbf{V},\boldsymbol{\eta}\right)_{\mathcal{G}_t}+\nu\left(\nabla\mathbf{V},\nabla\boldsymbol{\eta}\right)_{\mathcal{G}_t}+\sum_{i,j}\left(\sigma_{ij}(\mathbf{V}),\frac{\partial\eta_i}{\partial x_j}\right)_{\mathcal{G}_t}\\ &\quad -\left(P,\nabla\cdot\eta\right)_{\mathcal{G}_t}+\left(\nabla\cdot\mathbf{V},q\right)_{\mathcal{G}_t},\\ \mathbf{L}(\boldsymbol{\eta}) &= (\mathbf{f},\boldsymbol{\eta})_{\mathcal{G}_t}.\end{aligned}$$

Now, by multiplying the equation (3) by a test function $\phi\in\Lambda$, integrating over the domain $\mathcal{G}_t$ and using the Green's theorem, we obtain the weak formulation of the Spallart-Almaras turbulence one-equation model: Find $\tilde{\nu}:[0,T]\mapsto\Lambda$ such that for all $\phi\in\Lambda$ and for any time $t\in[0,T]$ the following equation holds

$$\left(\frac{D^{\mathcal{A}_t}\tilde{\nu}}{Dt}+(\mathbf{V}-\mathbf{w}_g)\cdot\nabla\tilde{\nu}+Y,\phi\right)_{\mathcal{G}_t}+\left((\nu+\tilde{\nu})\nabla\tilde{\nu},\nabla\phi\right)_{\mathcal{G}_t}=(G,\phi)_{\mathcal{G}_t}+\left(\frac{c_{b_2}}{\beta}(\nabla\tilde{\nu})^2,\phi\right). \quad (5)$$

2.3 STRUCTURE MODEL

A typical section airfoil (semichord b) in subsonic air flow is considered as shown in Figure 2. A trailing edge flap is hinged at $c_\beta\, b$ after the midchord. By h, α and β the plunging of the elastic axis, pitching of the airfoil and rotation of the flap is denoted, respectively (see Figure 3). The system motion generates unsteady aerodynamic lift $L=L(t)$, aerodynamic moment $M=M(t)$ and hinge moment $M_\beta=M_\beta(t)$. By k_h, k_α and k_β the spring constant of wing bending, wing torsional stiffness and flap hinge moment are denoted, respectively. The mass matrix is defined by the mass m and the moment of inertia I_α of the entire airfoil around the elastic axis. The flap moment of inertia around the hinge is denoted by I_β. The equations of motion for a flexibly supported rigid airfoil, read

$$\mathbb{M}\,\ddot{\mathbf{u}}+\mathbb{B}\dot{\mathbf{u}}+\mathbb{K}\,\mathbf{u}+\mathbf{f}_{NL}(\mathbf{u})=\mathbf{f}, \quad (6)$$

where

$$\mathbb{M} = \begin{pmatrix} m & S_\alpha & S_\beta \\ S_\alpha & I_\alpha & (c_\beta - e)bS_\beta + I_\alpha \\ S_\beta & (c_\beta - e)bS_\beta + I_\alpha & I_\beta \end{pmatrix}, \quad \mathbb{K} = \begin{pmatrix} k_h & 0 & 0 \\ 0 & k_\alpha & 0 \\ 0 & 0 & k_\beta \end{pmatrix},$$

$$\mathbb{D} = \begin{pmatrix} d_h & 0 & 0 \\ 0 & d_\alpha & 0 \\ 0 & 0 & d_\beta \end{pmatrix},$$

and $\mathbf{u} = (h, \alpha, \beta)^T$, $\mathbf{f} = (-L, M, M_\beta)^T$. By $\mathbf{f}_{NL}$ the nonlinear terms are denoted.

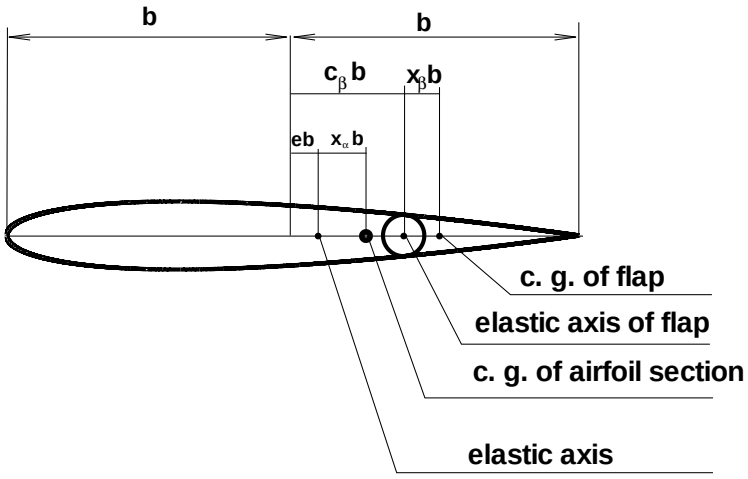


Figure 3: Typical airfoil section with three degrees of freedom.
By b the semichord of the airfoil is denoted, $e\,b$ denotes the location of the elastic axis of the wing after midchord, $x_\alpha\, b$ the location of the center of gravity after the elastic axis, $c_\beta\, b$ denotes the location of the flap hinge after the midchord and $x_\beta\, b$ the location of the center of gravity of the flap.

3 DISCRETIZATION OF THE PROBLEM

3.1 SPACE-TIME DISCRETIZATION

First, we start with time partition $0 = t_0 < t_1 < \cdots < T,\ t_k = k\Delta t$, with a time step $\Delta t > 0$ and approximate the function $\mathbf{V}(t_n)$, $P(t_n)$ and $\tilde{\nu}(t_n)$ defined in $\mathcal{G}_{t_n}$ at time t_n by $\mathbf{V}^n$, P^n and $\tilde{\nu}^n$. The ALE derivative can approximated by the finite differences

$$\left.\frac{D^{\mathcal{A}}\mathbf{u}}{Dt}\right|_{t^{n+1}} = \frac{3\mathbf{u}^{n+1} - 4\hat{\mathbf{u}}^n + \hat{\mathbf{u}}^{n-1}}{2\Delta t}, \qquad \left.\frac{D^{\mathcal{A}}\tilde{\nu}}{Dt}\right|_{t^{n+1}} = \frac{3\tilde{\nu}^{n+1} - 4\hat{\tilde{\nu}}^n + \hat{\tilde{\nu}}^{n-1}}{2\Delta t}, \tag{7}$$

where for a function $f : \mathcal{G}_i \mapsto R$ the function $\hat{f}^i : \mathcal{G}_{n+1} \mapsto R$ is defined as $\hat{f}^i = f \circ \mathcal{A}_{t_i} \circ \mathcal{A}_{t_{n+1}}^{-1}$ at a fixed time step t_{n+1}. Then the form $\mathbf{a}$ is modified in the following way:

$$\begin{aligned}
\mathbf{a}(\mathbf{b}; \mathbf{V}, P; \boldsymbol{\eta}, q) &= \left(\frac{3\mathbf{V}^{n+1}}{2\Delta t}, \boldsymbol{\eta}\right)_{\mathcal{G}_{n+1}} + \nu\Big(\nabla\mathbf{V}, \nabla\boldsymbol{\eta}\Big)_{\mathcal{G}_{n+1}} + \sum_{i,j}\left(\sigma_{ij}(\mathbf{V}), \frac{\partial \eta_i}{\partial x_j}\right)_{\mathcal{G}_{n+1}} \\
&\quad + \Big((\mathbf{b}\cdot\nabla)\mathbf{V}, \boldsymbol{\eta}\Big)_{\mathcal{G}_{n+1}} - \Big(P, \nabla\cdot\boldsymbol{\eta}\Big)_{\mathcal{G}_{n+1}} + \Big(\nabla\cdot\mathbf{V}, q\Big)_{\mathcal{G}_{n+1}}, \\
\mathbf{L}(\boldsymbol{\eta}) &= \left(\frac{4\hat{\mathbf{V}}^{n} - \hat{\mathbf{V}}^{n-1}}{2\Delta t}, \boldsymbol{\eta}\right)_{\mathcal{G}_{n+1}},
\end{aligned}$$

and the semi-implicit weak form of the Spallart-Almaras turbulence reads: Find $\tilde{\nu}^{n+1} \in \Lambda$ such that for all $\phi \in \Lambda$ holds the following equation

$$\mathbf{a}_{SA}(\tilde{\nu}^{n+1}, \phi) = \mathbf{L}_{SA}(\phi), \tag{8}$$

where

$$\mathbf{a}_{SA}(\tilde{\nu}^{n+1}, \phi) = \Big(\frac{3\tilde{\nu}^{n+1}}{2\Delta t} + (\mathbf{V}^{n+1} - \mathbf{w}_g)\cdot\nabla\tilde{\nu}^{n+1} + s^{(n)}\tilde{\nu}^{n+1}, \phi\Big)_{\mathcal{G}_{n+1}} + \Big(\frac{\nu + \tilde{\nu}^n}{\beta}\nabla\tilde{\nu}^{n+1}, \nabla\phi\Big)_{\mathcal{G}_{n+1}}$$

$$\mathbf{L}_{SA}(\phi) = \left(\frac{4\hat{\tilde{\nu}}^{n} - \hat{\tilde{\nu}}^{n-1}}{2\Delta t}, \phi\right)_{\mathcal{G}_{n+1}} + \Big(G^{(n)}, \phi\Big)_{\mathcal{G}_{n+1}} + \left(\frac{c_{b_2}}{\beta}(\nabla\hat{\tilde{\nu}}^{n})^2, \phi\right)_{\mathcal{G}_{n+1}},$$

and

$$s^{(n)} = c_{w_1}\frac{\tilde{\nu}^n}{y^2}\left(\frac{1 + c_{w_3}^6}{1 + c_{w_3}^6/g^6}\right)^{1/6}, \qquad G^{(n)} = c_{b_1}\overline{S}\hat{\tilde{\nu}}^{n}.$$

In order to apply the Galerkin FEM, we approximate the spaces W, X, Q from the weak formulation by finite dimensional subspaces $W_\Delta \subset W$, $Q_\Delta \subset Q$, $\Lambda_\Delta \subset \Lambda$ for $\Delta \in (0, \Delta_0)$ and we set

$$X_\Delta = \{\mathbf{v}_\Delta \in W_\Delta; \mathbf{v}_\Delta|_{\Gamma_D \cap \Gamma_{Wt}} = 0\}.$$

Hence, we define the *discrete problem* to find an approximate solution $\mathbf{V}_\Delta \in W_\Delta$ and $P_\Delta \in Q_\Delta$ such that $\mathbf{V}_\Delta$ satisfies approximately boundary conditions and the identity

$$a(\mathbf{V}_\Delta - \mathbf{w}_g; \mathbf{V}_\Delta, P_\Delta; \boldsymbol{\eta}_\Delta, q_\Delta) = \mathbf{L}(\boldsymbol{\eta}_\Delta), \qquad \text{for all } \boldsymbol{\eta}_\Delta, q_\Delta \tag{9}$$

The couple (X_Δ, Q_Δ) of the finite element spaces should satisfy the *Babuška-Brezzi (BB) inf-sup condition* (see, e.g. [7]). In our computations, the well-known Taylor-Hood P_2/P_1 conforming elements on triangular meshes are used for the velocity/pressure approximation.

The standard Galerkin discretization (9) may produce approximate solutions suffering from spurious oscillations for high Reynolds numbers. In order to avoid this drawback, the stabilization via *Galerkin Least-Squares technique* is applied (see, e.g. [5], [3]). The stabilization terms are defined as

$$\begin{aligned}\mathcal{L}_\Delta(\mathbf{b};\mathbf{V}_\Delta,p_\Delta;\boldsymbol{\eta}_\Delta,q_\Delta) &= \sum_{K\in\mathcal{T}_\Delta}\delta_K\left(\frac{3V_{\Delta\,i}}{2\Delta t}-\nu\triangle V_{\Delta\,i}+(\mathbf{b}\cdot\nabla)\,V_{\Delta\,i},(\mathbf{b}\cdot\nabla)\eta_{\Delta\,i}+\frac{\partial q_\Delta}{\partial x_i}\right)_K\\ &\quad+\sum_{K\in\mathcal{T}_\Delta}\delta_K\left(\frac{\partial P_\Delta}{\partial x_i}-\sum_{j=1}^{2}\frac{\partial\sigma_{ij}(\mathbf{V}_\Delta)}{\partial x_j},(\mathbf{b}\cdot\nabla)\eta_{\Delta\,i}+\frac{\partial q_\Delta}{\partial x_i}\right)_K,\\ \mathcal{F}_\Delta(\boldsymbol{\eta}) &= \sum_{K\in\mathcal{T}_\Delta}\delta_K\left(\frac{4\hat{V}^n_{\Delta\,i}-\hat{V}^{n-1}_{\Delta\,i}}{2\Delta t}+\mathbf{f}_i,(\mathbf{b}\cdot\nabla)\eta_{\Delta\,i}+\frac{\partial q_\Delta}{\partial x_i}\right)_K,\end{aligned}\tag{10}$$

and the additional grad-div stabilization terms

$$\mathcal{S}_\Delta(\mathbf{V}_\Delta,\boldsymbol{\eta}_\Delta)=\sum_{K\in\mathcal{T}_\Delta}\tau_K(\nabla\cdot\mathbf{V}_\Delta,\nabla\cdot\boldsymbol{\eta}_\Delta)_K,\tag{11}$$

are introduced with parameters $\delta_K\geq 0$ and $\tau_K\geq 0$

$$\delta_K\approx h^2,\qquad \tau_K\approx 1$$

The *stabilized discrete problem* reads: Find $\mathbf{V}_\Delta\in W_\Delta$ and $P_\Delta\times Q_\Delta$ such that $\mathbf{V}_\Delta$ satisfies approximately conditions (2), a), b) and

$$\begin{aligned}&\mathbf{a}(\mathbf{V}_\Delta-\mathbf{w}_g;\mathbf{V}_\Delta,P_\Delta;\boldsymbol{\eta}_\Delta,q_\Delta)+\mathcal{L}_\Delta(\mathbf{V}_\Delta-\mathbf{w}_g;\mathbf{V}_\Delta,P_\Delta;\mathbf{v}_\Delta,q_\Delta)\\ &+\mathcal{S}_\Delta(\mathbf{V}_\Delta,\boldsymbol{\eta}_\Delta)=\mathbf{L}(\boldsymbol{\eta}_\Delta)+\mathcal{F}_\Delta(V_\Delta)\qquad\text{for all }\boldsymbol{\eta}_\Delta\in X_\Delta,q_\Delta)\in Q_\Delta.\end{aligned}\tag{12}$$

Furthermore, the approximate solution of the RANS system (1) is coupled with the Spallart-Almaras turbulence model given by the solution of (8). The nonlinear algebraic discrete system (12) and (8) is solved on each time level t_{n+1} with the aid of the linearized Oseen iterative process. More detailed description of Oseen iterative process can be found in [9] for (laminar) Navier-Stokes equations.

4 MESH MOVING STRATEGY

For the mesh motion the linear elasticity analogy is used due to the robustness of this approach. The mesh is assumed to obey the linear elasticity equation, which can be written as

$$-\sum_j\frac{\partial\sigma_{ij}}{\partial x_j}=f_i,\qquad \sigma_{ij}=\lambda\left(\sum_k\varepsilon_{kk}\right)\delta_{ij}+2\mu\varepsilon_{ij},$$

and

$$\varepsilon_{ij}(\mathbf{u})=\frac{1}{2}\left(\frac{\partial u_i}{\partial x_j}+\frac{\partial u_j}{\partial x_i}\right).$$

The Lamé constants λ and μ are given by

$$\begin{aligned} \lambda &= \frac{E\sigma}{(1+\sigma)(1-2\sigma)} \\ \mu &= \frac{E}{2(1+\sigma)}, \end{aligned}$$

where E represents the modulus of elasticity and σ the Poisson ratio for a solid material. The vector $\mathbf{u} = (u_1, u_2)$ represents the displacement. The advantage of this approach is that regions of large modulus of elasticity E will be displaced as a solid body, see Figure 4. We employ a distribution of E which is inversely proportional to the cell volume, see [11]

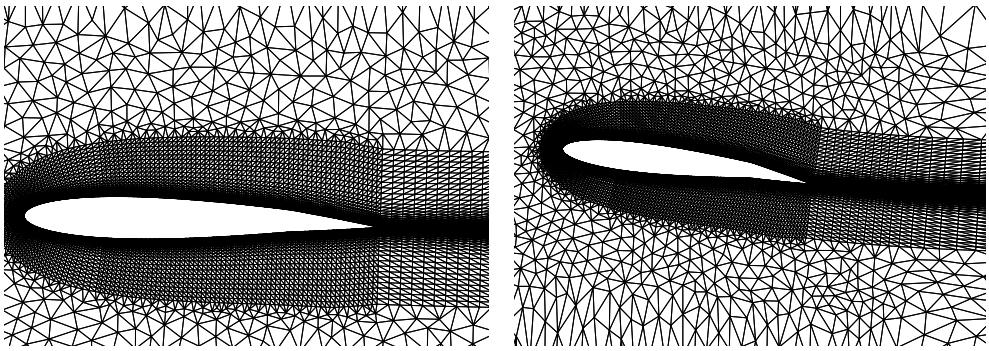


Figure 4: Grid deformation computed by the linear elasticity analogy for two different positions.

5 RESULTS OF AEROELASTIC COMPUTATIONS

In the presented numerical results we restrict ourselves onto the case of two degrees of freedom h and α, i.e. $\beta \equiv 0$. The system of ordinary differential equations is then described by

$$\begin{aligned} m\,\ddot{h} + S_\alpha\,\ddot{\alpha} + d_h\dot{h} + k_h\,h &= -L(t), \\ S_\alpha\,\ddot{h} + I_\alpha\ddot{\alpha} + d_a\dot{a} + k_\alpha\,\alpha &= M(t). \end{aligned} \tag{13}$$

5.1 Flexibly supported airfoil

This section presents results of the numerical simulation of flow induced vibrations obtained for the airfoil NACA $63_2 - 415$. The following quantities are considered: $m = 0.086622$ kg, $S_\alpha = 0.000779673$ kg m, $I_\alpha = 0.000487291$ kg m^2, $k_h = 105.109$ N m^{-1}, $k_\alpha = 3.695582$ N m rad^{-1}, $l = 0.05$ m, $b = 0.15$ m, $\rho = 1.225$ kg $^{-3}$, $\nu = 1.5 \cdot 10^{-5}$ m s^{-2}. The position of the elastic axis EA measured along the chord from the leading edge is $\mathrm{x}_{EA} = 0.8\,b = 0.12$ m, . We consider two different positions of the centre

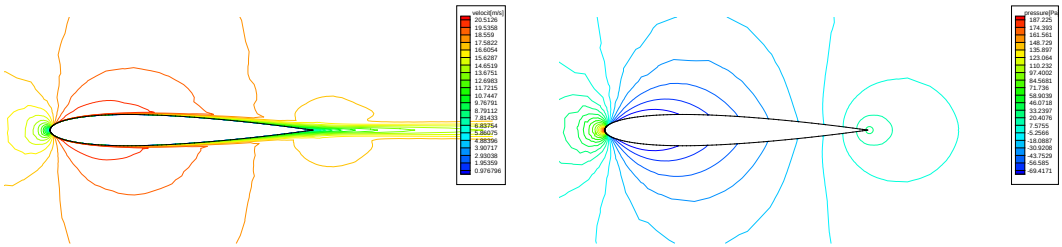


Figure 5: The time averaged fluid velocity and pressure isolines for inlet velocity $U = 25m\,s^{-1}$, stationary solution.

of gravity T measured along the chord from the leading edge $\mathrm{x}_T = 0.86b = 0.129$ m and $\mathrm{x}_T = 0.74b0.111$ m, which corresponds to choice $S_\alpha = 0.000779673$ and $S_\alpha = -0.000779673$, respectively. The structural damping is neglected and d_h and d_α are set to 0.

The far field flow velocity is considered in the range $U_\infty = 5\ -50\ \mathrm{m\,s}^{-1}$, which yields the Reynolds number $Re = U_\infty c/\nu$ in the range $10^5 - 10^6$. Although the numerical scheme presented above can be applied on any triangular mesh, accurate results are conditioned by the use of a mesh sufficiently refined in regions of strong gradients, e.g. in a boundary layer. The anisotropic mesh generator from [2] was employed for the adaptive mesh refinement and the resulting mesh was adapted to the solution behaviour.

First, we show the results for the case of $x_T = 0.74b$. Figure 5 show the velocity and pressure distribution for the far field velocity $U = 25m\,s^{-1}$, Figures 8 and 9 show the stable and unstable situation as well as the comparison with NASTRAN computations.

Next, for the case $x_T = 0.86b$ Figures 10, 11 shows the behaviour of the aeroelastic model with increasing far field velocity.

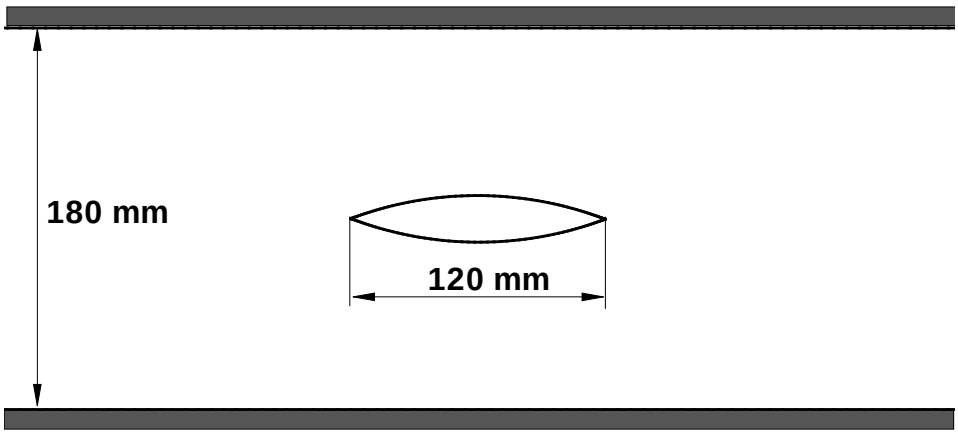


Figure 6: Channel configuration

$\boldsymbol{x_T}$	$0.86b$	$0.74b$
$\boldsymbol{S_\alpha}$	0.000779673 kg m,	-0.000779673 kg m,
critical flow velocity	30.3 $\mathrm{m\,s^{-1}}$	37.7 $\mathrm{m\,s^{-1}}$

Table 1: The results obtained by NASTRAN code (see [1])

5.2 Flexibly supported airfoil in a channel

This section presents results of the numerical simulation of flow induced vibrations obtained for the airfoil in the channel (Figure 6). The following quantities are considered: $m = 0.1$ kg,, $S_\alpha = -0.00013$ kg m, $I_\alpha = 0.000095$ kg m^2, $k_h = 1500$ N m^{-1}, $k_\alpha = 5.5$ N m rad^{-1}, $l = 0.08$ m, $b = 0.060$ m, $\rho = 1.225$ kg m^{-3}, $\nu = 1.5 \cdot 10^{-5}$ m s^{-2}. The position of the elastic axis EA of the airfoil measured along the chord from the leading edge is $\mathrm{x}_{EA} = \frac{2}{3}b = 0.4$ m . The damping coefficients d_h and d_α are set to $d_h = 5.0$ N s /m and $d_\alpha = 0.003$ N m s / rad.

The far field flow velocity is considered in the range $U_\infty = 0\ \mathrm{m\,s^{-1}} - 50\ \mathrm{m\,s^{-1}}$. Figure 12 shows the numerical results. The experimental critical velocity was $V_\infty \approx 120\mathrm{m}\ \ \mathrm{s}^{-1}$.

Acknowledgment
This research was supported under the project of the Grant Agency of the Academy of Science of the Czech Republic No IAA200760613 "Computer modelling of aeroelastic phenomena for real fluid flowing past vibrating airfoils particularly after the loss of system stability" and also under Research Plan MSM 6840770003 of the Ministry of Education of the Czech Republic.

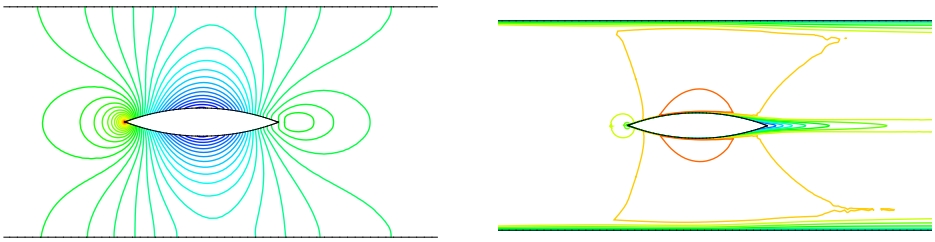


Figure 7: Numerical comparison with experiment. The airfoil with two degrees of freedom in the channel.

REFERENCES

[1] J. Čečrdle and J. Maleček. Verification FEM model of an aircraft construction with two and three degrees of freedom. Technical Report Research Report R-3418/02, Aeronautical Research and Test Institute, Prague, Letňany, 2002.

[2] V. Dolejší. Anisotropic mesh adaptation technique for viscous flow simulation. *East-West Journal of Numerical Mathematics*, 9 (1):1–24, 2001.

[3] T. Gelhard, G. Lube, and M. A. Olshanskii. Stabilized finite element schemes with LBB-stable elements for incompressible flows. *Journal of Computational Mathematics*, 177:243–267, 2005.

[4] P. LeTallec and J. Mouro. Fluid structure interaction with large structural displacements. In *4th ECCOMASS Computational Fluid Dynamics Conference*, pages 1032–1039, 1998.

[5] G. Lube. Stabilized Galerkin finite element methods for convection dominated and incompressible flow problems. *Numerical Analysis and Mathematical Modellin*, 29:85–104, 1994.

[6] T. Nomura and T. J. R. Hughes. An arbitrary Lagrangian-Eulerian finite element method for interaction of fluid and a rigid body. *Computer Methods in Applied Mechanics and Engineering*, 95:115–138, 1992.

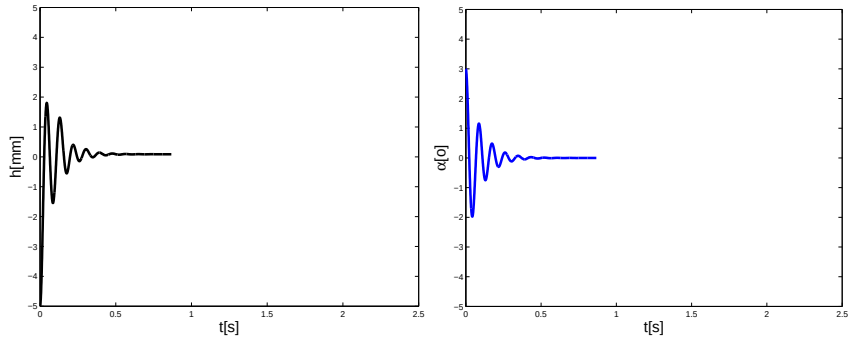
[7] V. Girault P.-A. Raviart. *Finite Element Methods for the Navier-Stokes Equations*. Springer, Berlin, 1986.

[8] P. Sváček and M. Feistauer. Application of a stabilized FEM to problems of aeroelasticity. In M. Feistauer, V. Dolejší, and Najzar K., editors, *Numerical Mathematics and Advanced Applications, ENUMATH2003*, pages 796–805, Heidelberg, 2004. Springer.

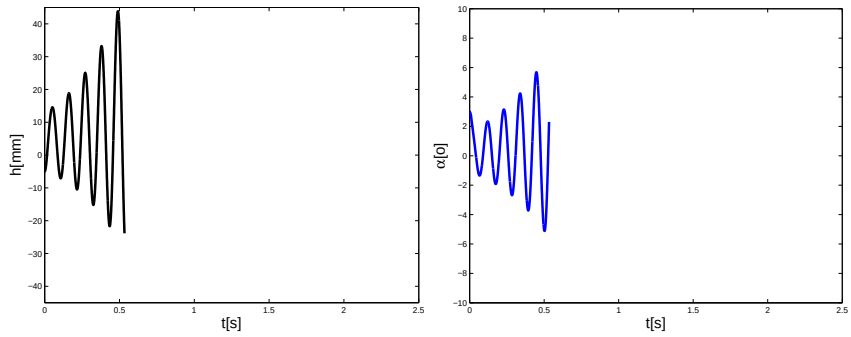
[9] Sváček, P. , M. Feistauer, and J. Horáček. Numerical simulation of flow induced airfoil vibrations with large amplitudes. *Journal of Fluids and Structures*, 2004. (submitted).

[10] D. C. Wilcox. *Turbulence Modeling for CFD*. DCW Industries, 1993.

[11] Zhi Yang and Dimitri J. Mavriplis. Unstructured dynamic meshes with higher-order time integration schemes for the unsteady Navier-Stokes eq uations. In *43rd AIAA Aerospace Sciences Meeting*, page 13 pp., Reno NV, January 2005. AIAA Paper 2005-1222.



$V_\infty = 25$ m s^{-1}



$V_\infty = 40$ m s^{-1}

Figure 8: The flexibly supported airfoil in free stream with the elastic axis located after the center of gravity measured from the leading edge of the airfoil.
RANS simulations with Spallart-Almaras turbulence model for $V_\infty = 25$ *and* 40 $m\ s^{-1}$. *The graph of the airfoil displacements in* h *(on the left) and* α *(on the right). For velocity* $V_\infty = 40m\ s^{-1}$ *you can see the typical flutter behaviour.*

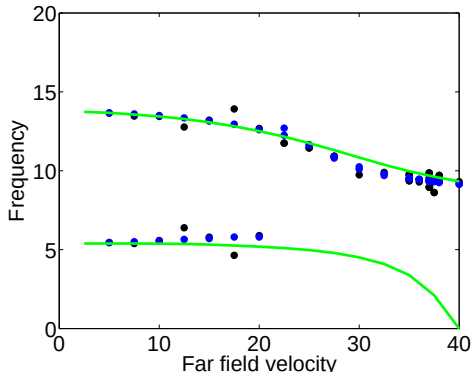


Figure 9: The flexibly supported airfoil in free stream with the elastic axis located after the center of gravity.
Comparison of the frequencies from computed signals to the frequency determined by NASTRAN computations.

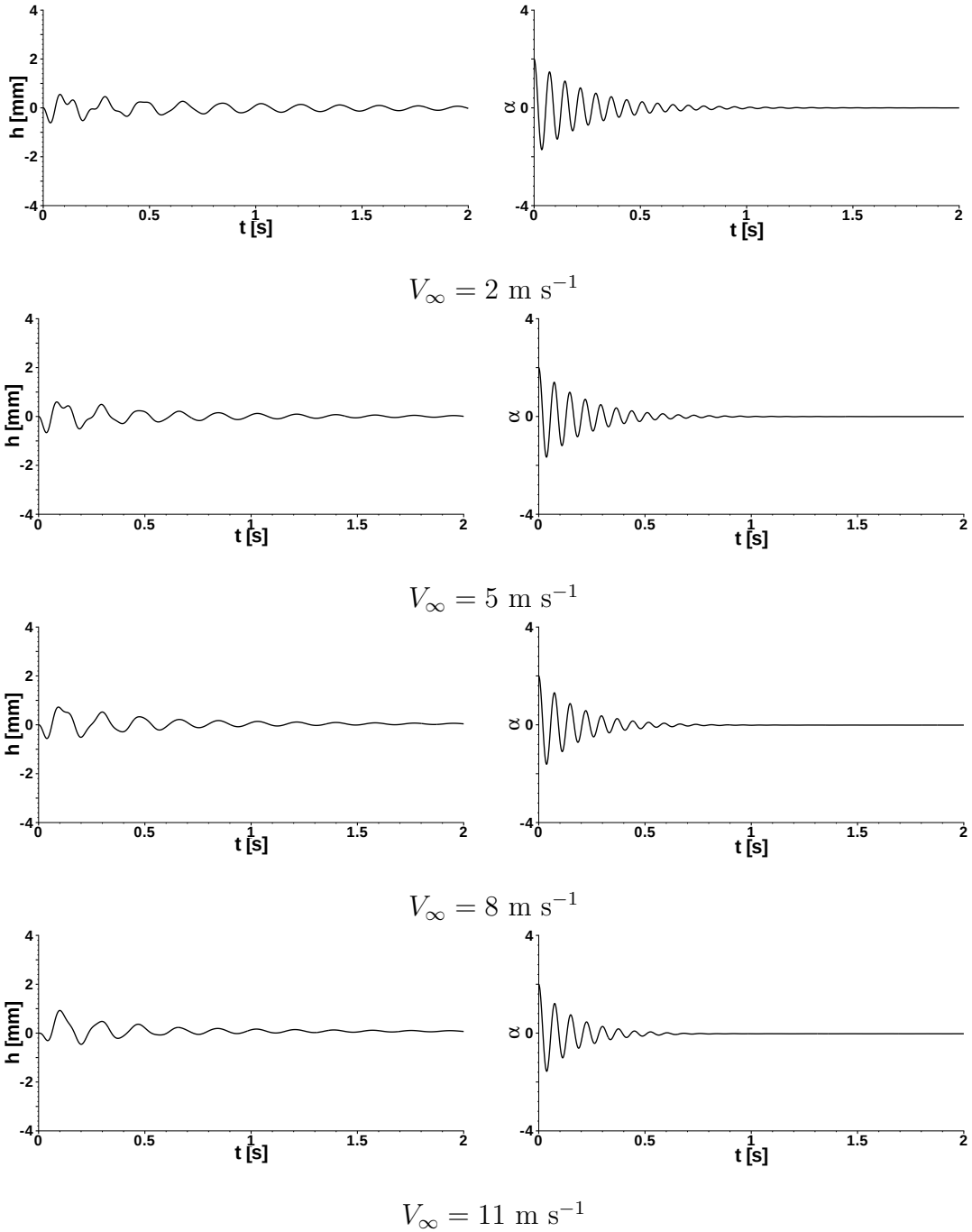


Figure 10: The flexibly supported airfoil in free stream with the elastic axis located front to the center of gravity measured from the leading edge of the airfoil.
RANS simulations with Spallart-Almaras turbulence model for $V_\infty = 2, 5, 8$ and 11 $m\ s^{-1}$ The graph of the airfoil displacements in h (on the left) and α (on the right). In this case the coupled model is in stable region and two main frequencies can be identified in the aeroelastic response of the airfoil. Futhermore, with increasing far field velocity the aerodynamical damping is increasing.

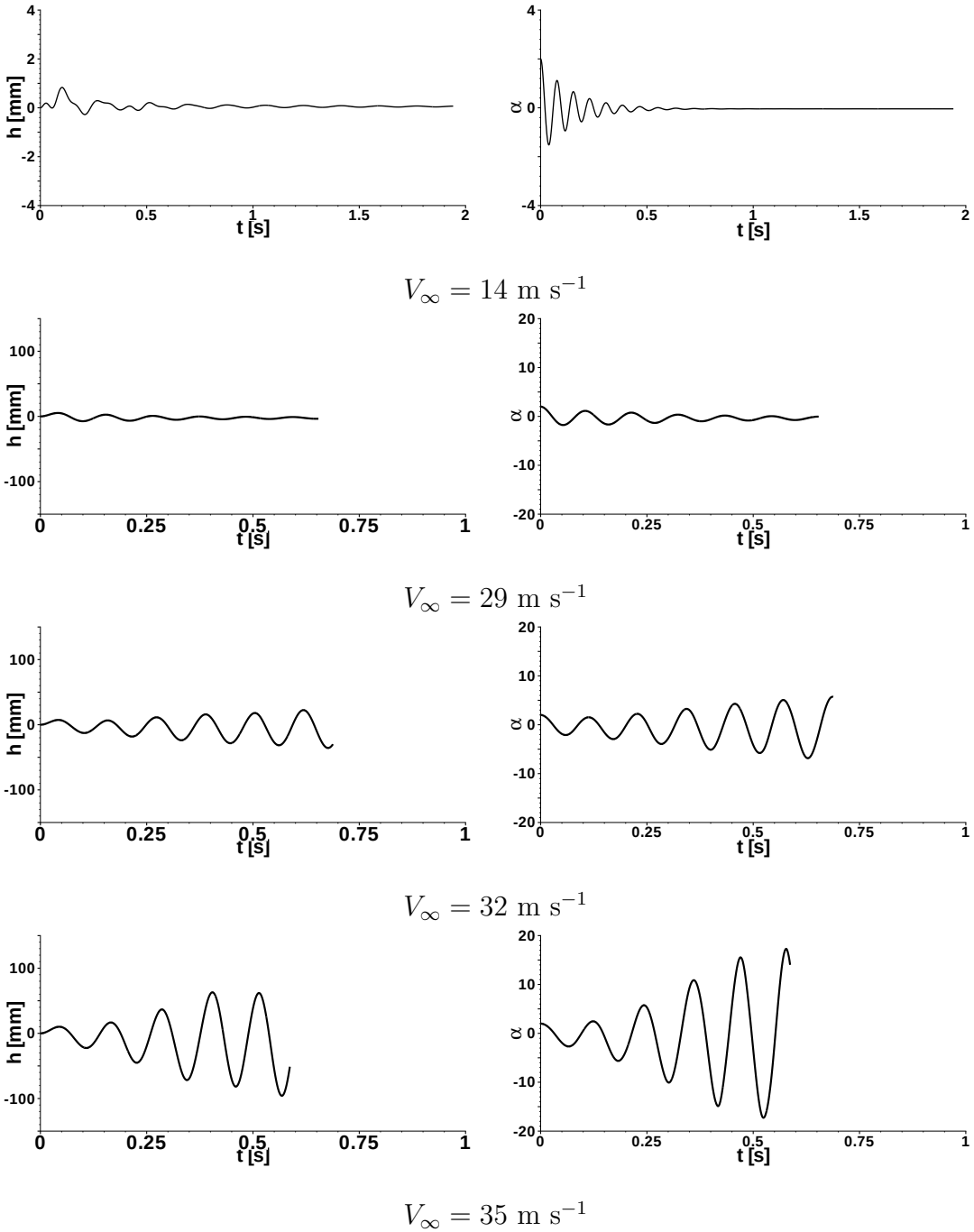


Figure 11: The flexibly supported airfoil in free stream with the elastic axis located front to the center of gravity measured from the leading edge of the airfoil.
RANS simulations with Spallart-Almaras turbulence model for $V_\infty = 14, 29, 32, 35$ m s^{-1} The graph of the airfoil displacements in h (on the left) and α (on the right). For $V_\infty = 35$ m s^{-1} the typical flutter behaviour can be observed.

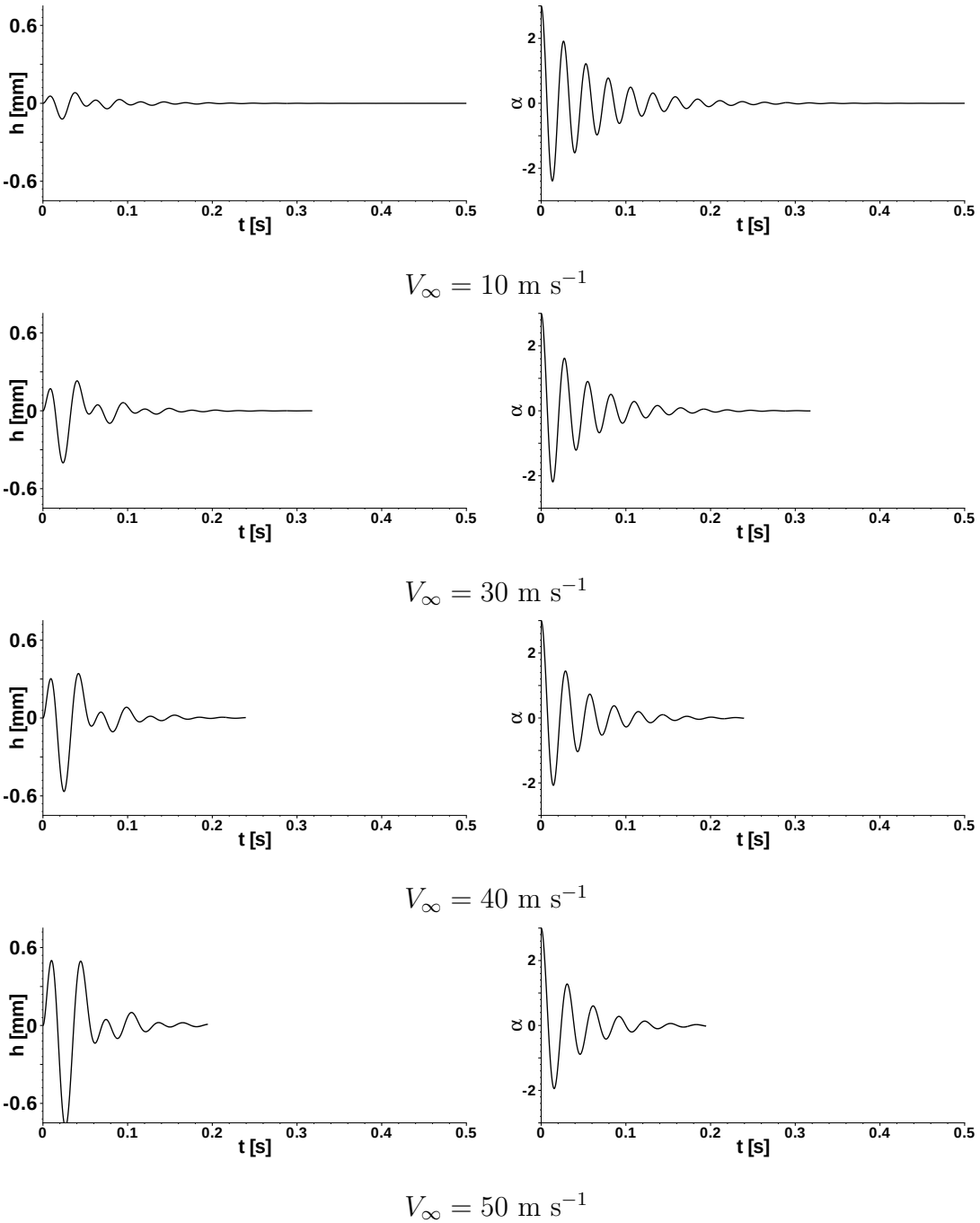


Figure 12: The flexibly supported airfoil in the channel.
RANS simulations with Spallart-Almaras turbulence model for $V_\infty = 10, 30, 40, 50$ m s^{-1}
The graph of the airfoil displacements in h (on the left) and α (on the right). In this case the coupled model is in stable region and two main frequencies can be identified in the aeroelastic response of the airfoil.